CELLULAR NEUROSCIENCE

Analysis of the bystander effect in cone photoreceptors via a guided neural network platform

Yuan Ma,[1,2,3] Xin Han,[1,3] Ricardo Bessa de Castro,[1,3,4] Pengchao Zhang,[1,3] Kai Zhang,[1,3] Zhongbo Hu,[2] Lidong Qin[1,3]*

The mammalian retina system consists of a complicated photoreceptor structure, which exhibits extensive random synaptic connections. To study retinal development and degeneration, various experimental models have been used previously, but these models are often uncontrollable, are difficult to manipulate, and do not provide sufficient similarity or precision. Therefore, the mechanisms in many retinal diseases remain unclear because of the limited capability in observing the progression and molecular driving forces. For example, photoreceptor degeneration can spread to surrounding healthy photoreceptors via a phenomenon known as the bystander effect; however, no in-depth observations can be made to decipher the molecular mechanisms or the pathways that contribute to the spreading. It is then necessary to build dissociated neural networks to investigate the communications with controllability of cells and their treatment. We developed a neural network chip (NN-Chip) to load single neurons into highly ordered microwells connected by microchannels for synapse formation to build the neural network. By observing the distribution of apoptosis spreading from light-induced apoptotic cones to the surrounding cones, we demonstrated convincing evidence of the existence of a cone-to-cone bystander killing effect. Combining the NN-Chip with microinjection technology, we also found that the gap junction protein connexin 36 (Cx36) is critical for apoptosis spreading and the bystander effect in cones. In addition, our unique NN-Chip platform provides a quantitative, high-throughput tool for investigating signaling mechanisms and behaviors in neurons and opens a new avenue for screening potential drug targets to cure retinal diseases.

INTRODUCTION

The structural and functional organization of the vertebrate retina is highly adapted for the initial sensing and processing of light signals, but its delicate structure also makes it vulnerable to dysfunction and diseases. The major causes of retinal diseases in adults are the progressive dysfunction and death of photoreceptors, which is induced by excessive light irradiation or mutations (Fig. 1A) (*1*). In most degenerative retinal diseases, such as retinitis pigmentosa and age-related macular degeneration, gap junction intercellular communication (GJIC) plays a critical role in the propagation of neuron degeneration and death via a phenomenon known as the bystander effect (*2*). This phenomenon—that parts of the retina degenerate and cause the deterioration of adjacent cells—severely affects neuron connections and synchronization, and gradually results in the loss of vision (*3*–*6*).

The role of the bystander effect in photoreceptor degeneration has been studied primarily in vivo, and the observations were made with tissue staining. Several studies have shown that mutations in the rod photoreceptors induce degeneration in adjacent cones, leading to a gradual loss of vision. The function of the photoreceptor gap junction coupling and its relation to the retina degeneration process are thus interesting to study (*4*, *5*). Besides, maintenance of cone functions can extend most of the visual capability in patients, even in those with degenerated rod photoreceptors (*7*, *8*). Therefore, it is important to dissect the bystander effect mechanisms between cones for potential therapeutic approaches.

In particular, the ability to study the bystander effect among photoreceptors in vitro has been limited by the lack of controllable models and quantitative analysis. In tissue experimental models, the apoptosis spreading and the bystander effect cannot be discriminated from the highly coupled photoreceptor layer (*9*). In most cases, toxic substances may transmit through gap junctions or diffuse into cells from the surrounding matrix, which is not easy to distinguish in tissue models (*4*). Therefore, new models are in urgent need so that such mysteries can be deciphered in a clear, precise, and controllable mode.

Micro- and nanotechnology platforms, which use precise fabrication techniques and the physical properties of flow and operate at the micrometer scale, provide enough precision and controllability for living cell study (*10*, *11*). These techniques should allow the production of a highly ordered neuron array and the high-throughput study of neural conduction or signal transmission between single neurons (*12*, *13*). Here, we developed a platform using a unique microwell array interconnected by microchannels that can rapidly load single neurons in a high-throughput, user-friendly manner (Fig. 1B). Although the microwell technology has been widely used in many biological systems, it is the first time that it is perfectly implemented to neural network study and bystander killing effect exploration. To study the bystander effect at the single-cell level, we loaded single neurons into microwells to isolate neural cell bodies. Each microwell was connected to the surrounding microwells with microchannels that allowed neural communications via their synapses. To our knowledge, this platform can achieve the highest efficiency in cell loading in an up-open system and with cultured cells on a chip. Because this device created a neural network guided by microchannels, we named it neural network chip, or NN-Chip.

To investigate the bystander effect in cones, we loaded cone photoreceptor–derived 661W cells onto the NN-Chip. The 661W cells express the blue and green opsins, cone pigments, and arrestin but no rod-specific antigens, which characterize the cell line as a proper cone model for the bystander effect study (*14*–*16*). We induced apoptosis using blue light irradiation and monitored the apoptosis propagation

[1]Department of Nanomedicine, Houston Methodist Research Institute, Houston, TX 77030, USA. [2]College of Materials Sciences and Optoelectronics, University of Chinese Academy of Sciences, Beijing 100049, China. [3]Department of Cell and Developmental Biology, Weill Cornell Medical College, New York, NY 10065, USA. [4]College of Engineering, Swansea University, Singleton Park, Swansea SA2 8PP, UK.
*Corresponding author. Email: lqin@houstonmethodist.org

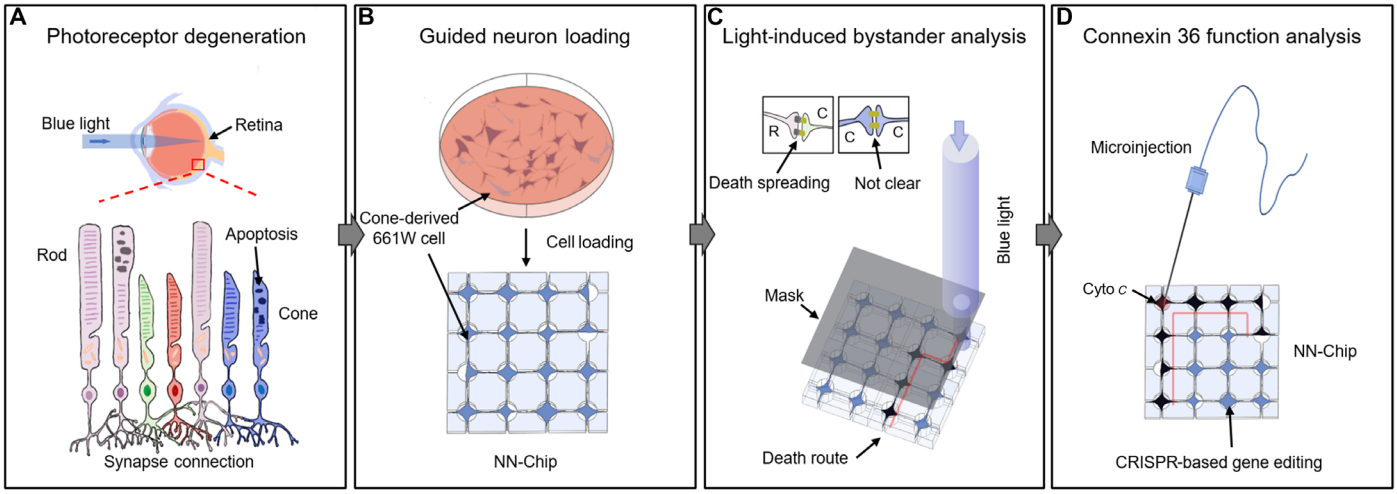

Fig. 1. Dissecting the mechanisms of photoreceptor degeneration via the bystander effect using the NN-Chip platform. (**A**) Excessive light irradiation induces apoptosis in photoreceptors, which are highly connected throughout the photoreceptor layer by random synapses. (**B**) To dissect photoreceptor communication, which is normally highly coupled in tissue and in dish culture, we loaded the 661W cells individually onto the NN-Chip. Each microwell was connected by microchannels to allow synapse formation between each photoreceptor, generating a highly guided neural network. (**C**) To study the bystander killing effect between cones, we selectively induced apoptosis using blue light sources. (**D**) To quantitatively analyze the role of Cx36 in bystander killing between cones on the NN-Chip, we used CRISPR (clustered regularly interspaced short palindromic repeats)–based gene-edited cells in conjunction with a microinjection unit.

(Fig. 1C). Using this clear and visualized system, we observed the apoptosis propagation between cones, which likely occurred due to the enhanced coupling via their connexin 36 (Cx36)–containing gap junctions (*17*). Next, to study the role of Cx36 in apoptosis, which is currently being debated (*18*, *19*), and the bystander effect, we used a microinjection unit in conjunction with our NN-Chip platform to perform Cx36 loss-of-function studies (Fig. 1D). Our data showed that Cx36 is required for the cone-to-cone bystander killing phenomenon and is also a deterministic factor for the range and speed that apoptosis can spread. Our study suggests that this structural gap junction protein could be a potential treatment target for alleviating cone photoreceptor degeneration.

RESULTS

Design and operation of the NN-Chip platform

The NN-Chip was designed with AutoCAD software and fabricated using photolithography and polydimethylsiloxane (PDMS) technologies. The device is made up of 2.25×10^4 uniform microwells distributed as a 150×150 array, and all adjacent wells were connected by microchannels. In typical microfluidic devices, cells are trapped and loaded using fluid control, whereas in our NN-Chip, we placed suspended cells on top of the NN-Chip and then loaded single cells into each well using programmed centrifugation (Fig. 2, A and B, and movie S1). We designed our device as an up-open stage to facilitate various treatments on cell throughout the experiment, which is indispensable for the bystander effect research. To use the NN-Chip to assess the bystander effect between cones, the device parameters were empirically optimized to meet the following conditions: (i) Only one cell is loaded into each microwell. (ii) Cells should remain in the same well, without migration, during the entire experiment. (iii) Neurons spread their protrusions along with the channels and are coupled with adjacent cells (Fig. 2C). The NN-Chip can also load cells of different types and sizes by sequentially centrifuging into the corresponding wells, allowing the study of various combinations of cell interactions in the future.

For the cone photoreceptor–derived 661W cells, we found the optimal microwell diameter to be 20 μm, the optimal channel width to be 3 μm, and the length to be 20 μm. To our knowledge, the NN-Chip has a higher cell-loading efficiency (>95% single-cell coverage) than single-cell microwell workstations used in previous reports (Fig. 2, D and E); moreover, this high-throughput platform is extremely suitable to study the bystander behavior (*20*). It should be noted that the arrayed pattern, the well diameter, and the channel width, length, and shape are required to be optimized for different cell types to achieve the highest loading efficiency (fig. S1). To prevent migration of the cultured cells, we coated Eagle's basal medium (BME) in the microwells and microchannels, but not on the rest of the chip surface (fig. S2). After the cells were loaded, they were incubated for 6 hours in the conditioned medium to promote attachment and synapse formation (Fig. 2, F and G, and movie S2). We also loaded iCell neurons onto the NN-Chip under another optimized condition. This induced pluripotent stem–derived primary neurons can create their uniform neural network with stable synapse coupling after culturing on the NN-Chip (Fig. 2H).

Finally, we equipped our NN-Chip platform with a high-resolution, multi-position microscope and a microinjection unit. This system permitted us to dissociate the complicated retina structure into a uniform network; moreover, the accompanying microinjection unit allowed chemical modification, and the high-resolution microscope enhanced our observation potential, thereby improving the ability to assess the bystander effect in photoreceptor degeneration.

Blue light irradiation–induced 661W cell apoptosis while culturing on the NN-Chip

Blue light induces more damage than other visible wavelengths in 661W cells (*21*). After blue light over-irradiation, excessive reactive oxygen species (ROS) are generated by the high level of oxidative stress, which induces damage to proteins, lipids, and DNAs and results in apoptosis (*22*, *23*). On the basis of this knowledge, we measured ROS concentration after irradiation of the 661W-containing NN-Chip under a 3000-lux-intensity blue light source or a white light source with the same intensity

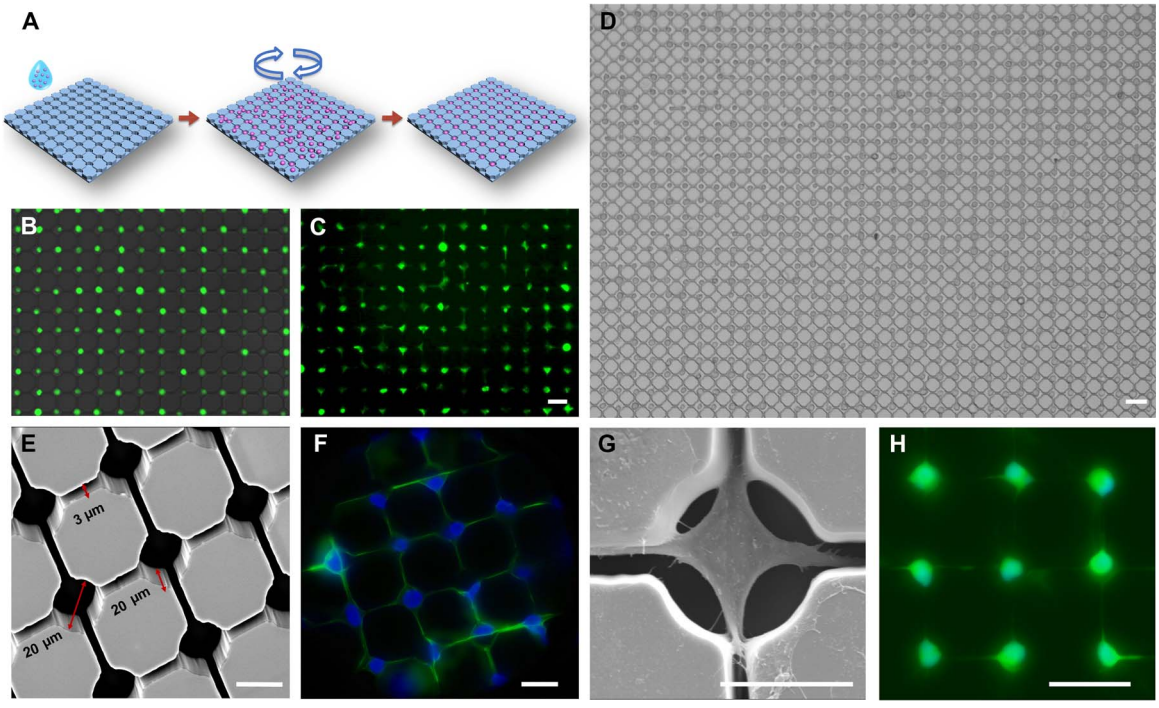

Fig. 2. Operation and design of the NN-Chip platform. (**A**) Schematic of the cell loading process. (**B**) Representative image of loading efficiency. The 661W cells were incubated in the medium with calcein for 20 min before loading. (**C**) Cell morphology after incubation for 1 hour on chip after loading. Scale bar, 40 μm. (**D**) Results of large-area loading by using the MDA-MB-231 cells with optimized parameters. Scale bar, 40 μm. (**E**) A scanning electron microscopy (SEM) image shows the neural network structure, including the microwells and their connecting microchannels, of the NN-Chip at a 30° tilt angle. (**F**) Representative images show that the 661W cells formed neural network on the NN-Chip. The actin (green) was labeled by phalloidin, and the nuclei (blue) was labeled with 4′,6-diamidino-2-phenylindole (DAPI). (**G**) A representative SEM image shows a 661W cell with synapses extending into the surrounding chambers along with the microchannel. (**H**) Neural network created by iCell neurons. Cells were stained by calcein after culturing on chip for 12 hours. Scale bar, 20 μm.

as control for various times. Using a dichlorodihydrofluorescein diacetate (H_2DCFDA) ROS probe, we found that ROS concentration increased significantly after 6 hours of blue light irradiation compared with that of white light (control) treatment (Fig. 3A). After 24 hours of blue light irradiation, ROS accumulation decreased, likely because most of the cells were completely dysfunctional. It is possible that, in the 661W cells, continuous blue light absorption increases ROS accumulation to the levels that exceed the cells' antioxidative ability, thus triggering apoptosis. ROS accumulation has also been shown to reduce the mitochondrial membrane potential (mmp), which plays an essential role in the antioxidant defense system (*24*). Thus, we evaluated the mmp of blue light–treated 661W cells using the JC-1 mmp assay, which labels healthy cells (with high mmp) red, because of the JC-1 aggregates, and apoptotic cells (with low mmp) green, because of the JC-1 monomers. The cells with red and green signals (merged) were considered as pre-apoptosis (Fig. 3B and fig. S3). We also used SYTOX Green to stain the apoptotic cells to verify the existence of the light-sensitive characteristics in the 661W cells while culturing on the NN-Chip. According to statistical data, with increasing blue light irradiation, the number of pre-apoptotic and apoptotic 661W cells increased (Fig. 3, C and D). This assay also demonstrated that blue light irradiation, and the accompanying increased ROS production, resulted in a significant mmp reduction in the 661W cells.

Short-wavelength opsin (S-opsin) is a light-sensitive, cone photoreceptor–specific protein that is, not surprisingly, highly expressed in the 661W cells (*25*). Some researchers have noted the S-opsin aggregation as an indicator of cone photoreceptor dysfunction after blue light irradiation (*26*). To determine whether this phenomenon occurs in our NN-Chip, we cultured the 661W cells on chip for 6 hours and then treated the cells with blue light for various times (fig. S4). S-opsin aggregation visibly increased after blue light treatment when compared with the white light group (Fig. 3E, arrows). Moreover, statistical results showed an increased percentage of S-opsin–aggregated cells in the 9- and 18-hour blue light–treated groups compared with those of the corresponding white light (Fig. 3F). Together, the increased ROS production, mitochondria dysfunction, and S-opsin aggregation that we observed after blue light irradiation demonstrated that the 661W cells, when cultured on our NN-Chip, maintain their previously documented light-sensitive properties; thus, the NN-Chip is a valid platform to study the bystander effect in the 661W cone photoreceptors.

Blue light–induced apoptosis spread to adjacent cells in a gap junction–dependent manner

To test the existence of bystander killing between cones, we first validated the existence of tight junctions in the connected synapses between adjacent 661W cells cultured on the NN-Chip (fig. S5). Then, a circular area with a radius of approximately 200 μm in the 661W-containing NN-Chip was treated for 6 hours using a 405-nm laser. After treatment, we removed the laser and monitored the apoptotic cell distribution by SYTOX Green staining. We monitored the results for up to 24 hours after irradiation, and it appeared that apoptosis had spread from the irradiated area to the adjacent cells. To determine whether apoptosis signals are transported to the adjacent cells via gap junctions, we added the gap junction blocker octanol (1 mM) to the culture medium (*27*);

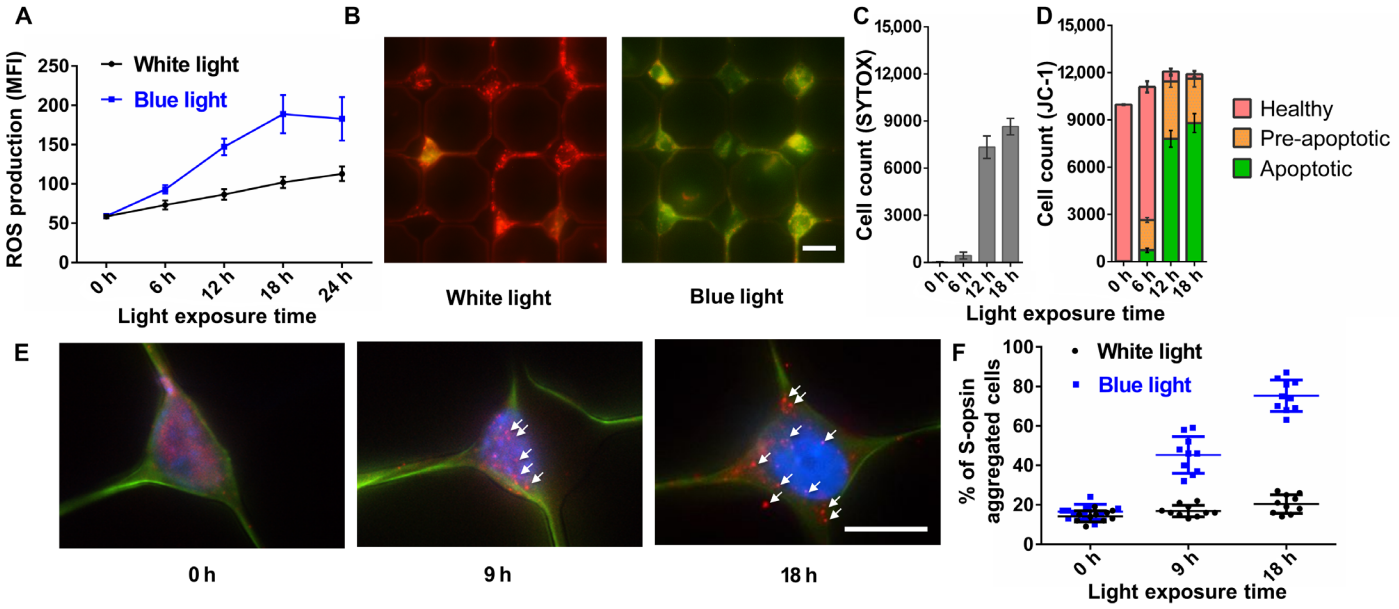

Fig. 3. Maintaining the blue light–sensitive characters of 661W cells after loading and culturing on the NN-Chip. (**A**) ROS production accumulation, as measured by the mean florescence intensity (MFI) of H_2DCFDA, was assessed following blue or white light irradiation for various times (n = 10). (**B**) Representative images show JC-1–stained 661W cells after blue light irradiation. The healthy cells with high mmp appeared red (aggregates), the apoptotic cells with low mmp appeared green (monomers), and the pre-apoptotic cells appeared red and green. Scale bar, 20 μm. (**C**) Number of the SYTOX Green–labeled cells under blue light irradiation for different time intervals. (**D**) Percentage of cells in each JC-1–stained group, which were counted in a 100 × 100 cell array (n = 10). (**E**) Representative immunostaining images show S-opsin aggregation in 661W cells on the NN-Chip after blue light irradiation for 9 and 18 hours. The cells were stained for actin [green fluorescent protein (GFP)] and S-opsin (Alexa Flour 647), and the nuclei were stained with DAPI. Scale bar, 20 μm. (**F**) Quantitative analysis showed that the percentage of S-opsin–aggregated cells was increased by blue light irradiation compared with that by white light irradiation.

this treatment appeared to ameliorate the spread of apoptosis during the 24-hour post-irradiation window. We also used quinine (50 μM) and meclofenamic (100 μM), which can selectively inhibit Cx36 and Cx43 individually to test the functions of different connexin types during the apoptosis propagation (*28*–*30*). Quinine also blocked apoptosis spreading, but meclofenamic did not. These results showed that, in cone photoreceptors, Cx36 plays a vital role in controlling apoptosis spreading, but Cx43 only slightly affects this phenomenon (Fig. 4A). We counted the apoptotic cells every hour after irradiation in each group. In the nontreated group, apoptosis increased throughout the time course; however, this increase was inhibited in the octanol- and quinine-treated group (Fig. 4B and movie S3). Together, all these data provided convincing evidence for the existence of a gap junction–dependent bystander killing effect manner between cone photoreceptors. In addition, Cx36, mainly expressed in the central neuron system especially in cones, could be a potential target for preventing the apoptosis spreading.

To assess the bystander killing effect at the single-cell level, we used a photomask with 1000 5-μm-radius transparent pinholes on top of the NN-Chip, which only allows blue light irradiation on only one cell each time. We first recorded the positions of the apoptotic cells after blue light irradiation. After that, we monitored the apoptotic cell distribution for various times and quantified the number of the post-apoptotic cells adjacent to the original ones. Time-lapse microscopy revealed that apoptosis eventually occurred in cells adjacent to the blue light–treated cells (Fig. 5A and movie S4). Next, we quantified the apoptotic cell distribution across the NN-Chip after blue light irradiation. We found that 80% of the subsequent apoptotic cells were adjacent to the originally treated ones, whereas the remaining apoptotic cells seemed to reflect as random apoptotic behavior (fig. S6). To further address the mechanism, we hypothesized that, if apoptosis spreads via paracrine, the apoptotic cells should be distributed uniformly around the blue light–treated cells, whereas if apoptosis spreads via gap junctions, the apoptotic cells should be distributed asymmetrically. To distinguish between these two scenarios, we counted the number of post-apoptotic cells adjacent to each pretreated cell. Most pretreated cells were only adjacent to one or two apoptotic cells (Fig. 5B), implying that apoptosis propagation is occurring directionally, likely via gap junctions, and not uniformly as paracrine. Finally, these results demonstrated the existence of the bystander killing effect in cone-derived 661W photoreceptors. Because cones are critical for color recognition and high visual acuity (*31*), treatments that inhibit this gap junction–mediated bystander effect between cones could extend the visual capabilities in some retinal disease patients with cone photoreceptor degeneration.

Cx36 is required for apoptosis spreading in cone photoreceptors

Gap junctions allow the passage of substances less than 1 kDa, such as Ca^{2+}, inositol trisphosphate, and adenosine triphosphate; however, the exact role of the gap junction protein Cx36 in the cone bystander killing effect remains controversial (*9*, *17*–*19*, *32*–*34*). On the basis of our results that Cx36 may have crucial functions in death signal transportation in cones, we then targeted this gap junction using a more straightforward method: by knocking out Cx36 in the 661W cells (Fig. 6A and fig. S7). Next, we used a microinjection unit to inject cytochrome c into single Cx36-knockout (KO) and wild-type (WT) 661W cells cultured on the NN-Chip to measure the apoptosis spreading results. In the cytoplasm, with the release of cytochrome c, several downstream apoptotic signals

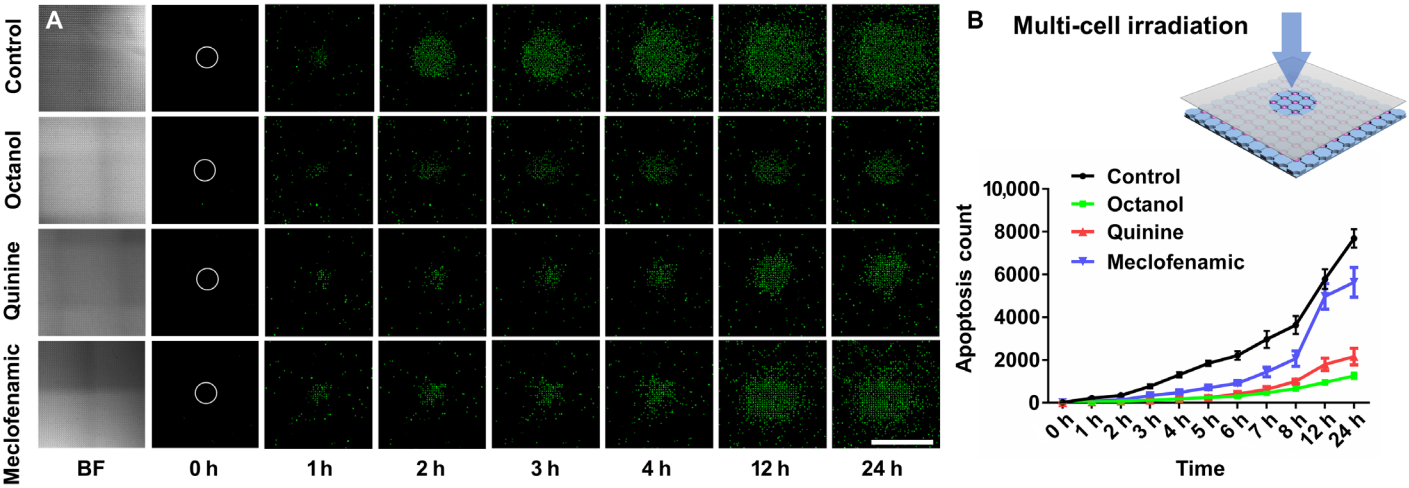

Fig. 4. Evidence of the gap junction–mediated bystander killing effect in the 661W cells. (**A**) Representative bright field (BF) and fluorescence images show apoptosis distribution, detected by SYTOX staining, in different gap junction inhibitors (octanol, 1 mM; quinine, 50 μM; meclofenamic, 100 μM) after 6 hours of blue light irradiation on the 661W-containing NN-Chip. White circles represent the initial irradiated area. Scale bar, 1 mm. (**B**) Schematic of the 405-μm laser spot diameter irradiation of the NN-Chip. Apoptosis was counted every hour for 24 hours after blue light irradiation (n = 10).

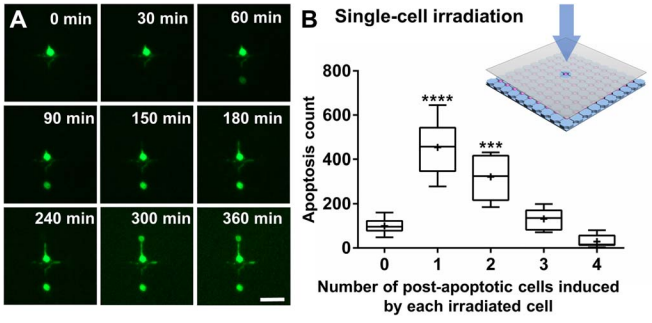

Fig. 5. Analysis of the bystander killing phenomenon at the single-cell level. (**A**) Representative time-course images of the bystander effect at the single-cell level in SYTOX-stained 661W cells on the NN-Chip. A single cell was irradiated to blue light, and two adjacent cells eventually undergo apoptosis. Scale bar, 40 μm. (**B**) Schematic of the 5-μm laser spot irradiation of the NN-Chip. The number of post-apoptotic cells induced by each pretreated cell was quantified. The whiskers go down to the smallest value and up to the largest. $P < 0.0001$ by one-way analysis of variance (ANOVA) analysis compared with zero- and four-cell group; n = 10.

are activated. Compared with light irradiation, both methods can trigger cell apoptosis, but cytochrome c acts as a more direct factor (*35*). Therefore, we chose the microinjection of cytochrome c, instead of light irradiation, to standardize the apoptosis time at the single-cell level.

Before performing the cytochrome c microinjection experiments, we optimized the experimental parameters. First, to minimize cell damage and satisfy that cells can still keep their normal function after injection, we optimized the injection pressure to 60 hPa, compensation pressure to 30 hPa, and injection time to 0.1 s (Fig. 6B and fig. S8) (*36*). Next, because only substances less than 1 kDa can pass through gap junctions, we verified gap junction function in our 661W-containing NN-Chip by injecting tracers of different molecular weights and monitoring their spread into adjacent cells. We injected solutions containing 100 mM Lucifer yellow (457 Da) and 100 mM fluorescein isothiocyanate (FITC)–dextran (10 kDa), and then analyzed their spreading after 15 min. Lucifer yellow, but not FITC-dextran, easily passed through the gap junctions into adjacent cells (Fig. 6, C and D). Similarly, after injection of both Lucifer yellow and Cascade blue dextran (3 kDa) into the same cell, Lucifer yellow, but not blue dextran, was observed in adjacent cells (Fig. 6, E and F). These data suggest that the gap junctions are functional between the 661W cells on the NN-Chip. These results are consistent with previous reports that showed that only substances less than 1 kDa can pass through the gap junctions (*37*).

After optimization, we mixed cytochrome c (10 mg/ml) and blue dextran (20 mg/ml) in microinjection buffer and injected it into the Cx36-KO and WT 661W cells; after 30 min, we cultured them in the SYTOX Green–containing medium. After 6 hours, we assessed the apoptosis and dextran spreading results. The Cx36-KO cells showed visibly less cell apoptosis spreading compared with the WT cells, and the dextran spreading patterns were similar to those of SYTOX in both groups (Fig. 6, G to J). In addition to the gap junctions remaining open after cell apoptosis, the gap junctions may be dysfunctional because of the loss of membrane integration during the bystander killing process, leading the blue dextran spread to the adjacent cells to form this similar pattern (*38*, *39*). Finally, we quantified apoptosis in cells adjacent to the cytochrome c–microinjected cells and demonstrated that the injected Cx36-KO cells had fewer adjacent cells undergoing apoptosis than the injected WT cells (Fig. 6K). These data suggest that Cx36 is responsible for the gap junction–dependent bystander effect in cone photoreceptors.

In summary, although inhibition of Cx36 may relieve the bystander effect in retinal diseases, Cx36 also provides many important functions in the retinal system (*32*, *33*, *40*), making it difficult to completely block Cx36 as a retinal protection mechanism (*41*). Thus, in the future, we aim to elucidate the importance rank of specific death signals, such as ion and microRNAs involved in the bystander effect, using the NN-Chip combined with the microinjection technologies; this should reveal a more feasible method to remedy cone photoreceptor degeneration.

DISCUSSION

Considerable research efforts have focused on finding the molecular mechanisms underlying the bystander effect, with most studies focusing on the role of connexins and gap junctions. Treating cells and observing

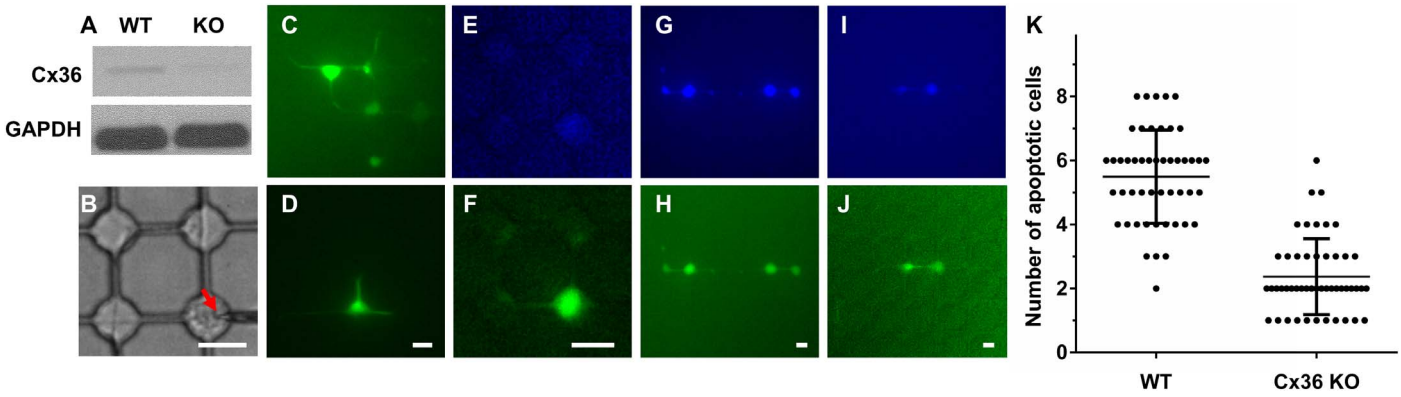

Fig. 6. Assessing the effects of Cx36 on apoptosis spreading in the 661W cells. (**A**) Western blot analysis shows loss of Cx36 in Cx36-KO cells relative to that in WT cells. Glyceraldehyde-3-phosphate dehydrogenase (GAPDH) was used as a loading control. (**B**) A cell was being injected with a Femtotip (inner diameter, 0.5 μm; outer diameter, 1 μm; Eppendorf) on the NN-Chip. (**C** and **D**) Dye distribution in 15 min after injection of 100 mM Lucifer yellow (457 Da) in (C) or of 100 mM FITC-dextran (10 kDa) in (D). (**E** and **F**) Dye distribution in 15 min after the injection of blue dextran (3 kDa) (E) and Lucifer yellow (F) and into the same cell. (**G** and **H**) Representative images show blue dextran (G) and SYTOX (H) distribution 6 hours after cytochrome c (10 mg/ml) and blue dextran (20 mg/ml) co-injection into a single WT cell. (**I** and **J**) Representative images show blue dextran (I) and SYTOX (J) distribution 6 hours after cytochrome c (10 mg/ml) and blue dextran (20 mg/ml) co-injection into a single Cx36-KO cell. (**K**) Quantitative analysis of apoptosis in WT and Cx36-KO groups. The results are calculated from 50 single-cell injections per group. Scale bars, 20 μm (B to J).

the behavior of adjacent cells have been the general methods used to dissect the mechanism of the bystander effect. However, researching the bystander killing effect at the single-cell level is a more recent trend that can uncover biological signals without the influence of uncertain elements associated with the complex structure and organization of neural networks. To date, photoreceptor bystander research is fraught with technical challenges, including difficulties in dissociating retinal structures and quantitatively measuring bystander killing speed, unclear observations, and the lack of a reliable single-cell assay. Thus, the ability to observe and quantify the bystander killing effect in cone photoreceptors is instrumental for further mechanistic research.

Here, we developed an innovative NN-Chip platform capable of high-efficiency cell loading via a user-friendly centrifugation method, allowing the immobilization of single cells in individual microwells; the cells are connected to adjacent cells via synapses at uniform distances. Furthermore, because our NN-Chip is an up-open platform combined with a microinjection unit, we can quickly treat single cells and assess the effects on adjacent ones. Using this platform, we demonstrated several findings regarding the bystander effect in cone photoreceptors. First, we established the existence of the bystander killing effect between cone photoreceptor–derived 661W cells by showing that blue light–induced apoptosis in one cell can directionally spread to adjacent cells. In our opinion, we have provided strong, clear, and, most importantly, quantitative evidence of a cone-to-cone bystander killing phenomenon. Second, we assessed the role of the gap junction protein Cx36, which is highly expressed in cones as a communication channel, in bystander killing phenomenon. Disruption of Cx36 via CRISPR-Cas9 (CRISPR-associated protein 9 nuclease) gene editing greatly decreased the apoptosis spreading compared with that of WT 661W cells. These data suggest that, in the cone photoreceptor layer, Cx36-containing channels act as tunnels that allow the passage of apoptotic signals between cone photoreceptors, thus propagating apoptosis throughout the entire photoreceptor layer.

In retina degeneration diseases, the bystander effect is an established mechanism to dissect apoptosis propagation from dying cells to healthy neighbors (*4*). As researches show, the gap junction provides a transmitting channel for toxic substances from dying rods to healthy cones (*10*), and we consequently analyzed the secondary bystander effect between cones. On the basis of our results that Cx36 provides an avenue for toxic spreading, we may conclude that, although the Cx36-based GJIC is not the only method between cones, Cx36 truly regulates the transmission of toxicity elements. Recently, the use of gene therapies and combined approaches has provided promising therapeutic perspectives; thus, Cx36 may provide a potential treatment target to delay the spreading of photoreceptor degeneration.

In conclusion, we created a novel platform for high-efficiency patterning of neural networks, combined with a microinjection unit, which we believe will lessen the challenges for dissecting the mechanisms of the bystander effect and gap junction functions. Moreover, this platform should have additional applications in other types of neuron studies.

MATERIALS AND METHODS

Cell culture

The 661W photoreceptor cell line was provided by M. Al-Ubaidi (Department of Biomedical Engineering, University of Houston). These cells were routinely cultured in Dulbecco's modified Eagle's medium (Gibco) supplemented with 10% heat-inactivated fetal bovine serum (Thermo Fisher Scientific) and 1% antibiotic-antimycotic (Gibco, 15240-062) with hydrocortisone 21-hemisuccinate (40 ng/ml; Sigma, H-2270), progesterone (40 ng/ml; Sigma, P-8783), putrescine (0.032 mg/ml; Sigma, P-7505), and 0.004% (v/v) β-mercaptoethanol (Sigma, M-6250) at 37°C in a humidified atmosphere with 5% CO_2. We used the conditioned medium (medium cultured with 661W cells for 6 hours) to culture cells on BME (Sigma)–coated NN-Chips. We cultured the iCell neurons (Cellular Dynamics International Inc.) onto the poly-L-ornithine/laminin (Sigma) surface-coated NN-Chip in the complete iCell neuron maintenance medium also at 37°C in a humidified atmosphere with 5% CO_2.

Design and fabrication of the NN-Chip mold

All designs were drawn with AutoCAD software and loaded as glass photomasks (Photo Sciences Inc.). PDMS devices were fabricated by standard photolithography and elastomer molding. We used SU-8 3025 negative photoresist (MicroChem Corp.) to fabricate the 20-μm-deep structures. The SU-8 3025 photoresist was spin-coated onto a 12.7-cm

silicon wafer at 500 rpm (Laurell Technologies Corp., model WS-400B-6NPP/LITE/AS) for 10 s with an acceleration of 100 rpm/s to spread out the photoresist and then at 3500 rpm for 60 s with an acceleration of 500 rpm/s. After soft baking at 65°C for 3 min and hard baking at 95°C for 10 min, the wafer was exposed under ultraviolet light with an exposure dose of 150 mJ/cm^2 for 3 s. It was then heated for post-exposure baking at 65°C for 1 min and hard baking at 95°C for 3 min. After 135°C heating for 30 min, the wafer was hydrophobic-processed by trimethylchlorosilane for 30 min. The modified wafer served as an SU-8 mold structure. The PDMS oligomer and cross-linking pre-polymer of the PDMS agent from a Sylgard 184 kit (Dow Corning) were mixed in a weight ratio of 10:1. After degassing in vacuum, the appropriate weight mixture was poured onto the SU-8 mold to form a 2-mm-thick layer and cured at 85°C for 40 min. After the PDMS replica was peeled off from the SU-8 mold, we cut the PDMS into several 6 × 6 mm squares. For better imaging and cell culturing method, we bonded the PDMS flat surface side to 12-mm glass-based 35-mm dish (Thermo Fisher Scientific) by oxygen plasma [1 min at an oxygen flow rate of 20 SCCM (standard cubic centimeter per minute), a chamber pressure of 500 mtorr, and a power of 50 W].

Operation of the NN-Chip

To load cells into the NN-Chip, we used the Sorvall Legend X1R Centrifuge (Thermo Fisher Scientific). First, we treated the NN-Chip surface by oxygen plasma (1 min at an oxygen flow rate of 20 SCCM, a chamber pressure of 500 mtorr, and a power of 50 W), immediately covered it with a BME droplet, and placed it at 37°C for 1 hour. After coating, we swiped the excessive liquid and moved the surface onto a 95°C digital dry bath (Bio-Rad) for 1 s to denature the BME coated on the surface. Once finished, we used a Staples invisible tape to peel off the excessive BME. After surface modification, we dropped the 20-μl medium containing suspended cells onto the surface of NN-Chip. We tested several spinning modes and chose the programmed centrifugation as follows: (i) 0 to 1000 rpm, acceleration = 1; (ii) 1000 rpm for 1 min; (iii) 1000 to 600 rpm, deacceleration = 1; (iv) 600 to 0 rpm, deacceleration = 9. After spinning, we transferred the NN-Chip to an inverted microscope (EVOS) and used filter papers (Whatman) from one side to swipe away the unloaded cells. Finally, we slightly dropped the 20-μl conditioned medium on the NN-Chip and cultured cells at 37°C in a humidified atmosphere with 5% CO_2. All the operations were finished in a culture hood to prevent contamination.

Creating the cone photoreceptor network

Loading single 661W cells with high efficiency is crucial for this high-throughput, single neural network platform. Correctly sizing the wells to match the 661W cell size largely influenced the loading efficiency. Efficiency improved as the well diameters increased from 20 to 30 μm; however, well diameters >30 μm increased the chance of two-cell loading. The density of the suspended cells also affected the loading efficiency, which was decreased by low density and cell gathering. Finally, we optimized the distance between the 661W cells to ensure high coupling of their synapses. We found that 40 μm between the center of every well was the optimal distance to ensure synapse coupling, without large-cell membrane contact. After all these optimizations, we routinely obtained a loading efficiency of >95%.

Cell staining

To have a better image, we used calcein (Thermo Fisher Scientific) to stain live cells. Cells were cultured in the calcein-containing medium (1 μM) for 30 min and then loaded onto the NN-Chip. Stained cells can keep the fluorescence for around 1 hour (fig. S1). We also used phalloidin (A12379, Invitrogen) to label the actin in the 661W cells.

Light treatment to the 661W cells

We used two kinds of blue and white light sources to treat cells under 3000-lux-intensity conditions. Cells were first loaded onto the NN-Chip and incubated under a humidified atmosphere of 5% CO_2 at 37°C. Then, they were treated with blue light-emitting diode (LED; 464 nm) or laser diode (405 nm) light on top of the NN-Chip, and the intensities were adjusted to the same lux using the Extech LT300 light meter (FLIR Commercial Systems Inc.). Control cells were incubated under the same intensity white LED light (the wavelength peaks are 456 and 553 nm) with the same humidity and temperature environment.

Measurement of cellular ROS production and mmp

For ROS production measurements, 661W cells were loaded onto the NN-Chip and cultured for 6 hours. After 6, 12, 18, or 24 hours of blue or white light irradiation, we added 10 μM CM-H_2DCFDA (Invitrogen) to the culture medium and incubated for an additional hour. CM-H_2DCFDA fluorescence was measured using a microplate reader (M33089, Thermo Fisher Scientific). Mmp was measured after the 661W cells were exposed to blue light for 6, 12, or 18 hours using the JC-1 Mitochondrial Membrane Potential Assay Kit (ab11850, Abcam). The images were captured using a fluorescence microscope (EVOS FL Auto Cell Imaging System), and the numbers of fluorescent cells (red, green, and merged) were counted using ImageJ.

Immunostaining

The 661W cells were loaded onto the NN-Chip and incubated for various times. For S-opsin immunostaining, we fixed the cells with 4% paraformaldehyde (Sigma) for 10 min and blocked them in 3% bovine serum albumin (Sigma) for 30 min after blue light irradiation. Then, we incubated the fixed cells overnight at 4°C with the primary antibody (sc-14363, Santa Cruz Biotechnology Inc.). After washing, the cells were incubated for 1 hour with the secondary antibody [donkey anti-goat immunoglobulin G (IgG) H&L (Alexa Fluor 647), Abcam]; then, cell nuclei were stained with DAPI. For Cx36 immunostaining, we used the same procedure with the following antibodies: Cx36 polyclonal antibody (Invitrogen), claudin-1 polyclonal antibody (Invitrogen, 71-7800), and goat anti-rabbit IgG H&L (Alexa Fluor 647, Abcam). Images were taken using a Nikon A1 confocal microscope.

Cell apoptosis analysis

SYTOX Green Dead Cell Stain (Thermo Fisher Scientific) was used to measure apoptosis levels in 661W cells. Medium containing SYTOX (0.5 μM) was added to the NN-Chip after blue light treatment to stain the nucleotides of dead cells; then, we observed apoptosis spreading by time-lapse microscope. To verify the SYTOX results, we used the Annexin V-FITC Apoptosis Detection Kit (Abcam) per the manufacturer's instructions. Dead cells were counted using ImageJ.

Generation of Cx36-KO 661W cells

The 661W cells were cultured in six-well plates at a density of 5 × 10^4 cells per well for 24 hours. Then, we added 2 μg of CRISPR/Cas9–Cx36-KO plasmid with a GFP reporter (sc-420563, Santa Cruz Biotechnology) and 6 μl of FuGENE HD Transfection Reagent (Promega) complex to 100 μl of Opti-MEM (Gibco). This transfection reaction was added to the culture medium, and after 24-hour incubation, we sorted the GFP-expressing

cells by flow cytometry (LSRFortessa, BD Biosciences). Then, we expanded these cells as single-cell colonies to screen for Cx36-KO 661W cells.

Western blotting analysis

The control and Cx36-KO 661W cells were seeded at a density of 5×10^5 cells per well in six-well plates and incubated for 24 hours. Then, the cells were washed with phosphate-buffered saline, lysed in radioimmunoprecipitation assay buffer (Sigma), and harvested. Lysates were centrifuged at 12,000 rpm for 10 min at 4°C. The protein concentrations were measured using the BCA Protein Assay Kit (Thermo Fisher Scientific) with standard bovine serum albumin. The samples were boiled for 10 min at 100°C. The proteins were separated by SDS–polyacrylamide gel electrophoresis gradient electrophoresis and transferred to polyvinylidene difluoride membranes (Bio-Rad). We used goat anti-Cx36 (sc-14904, Santa Cruz Biotechnology) as the primary antibody and horseradish peroxidase–conjugated donkey anti-goat IgG (ab97110, Abcam) as the secondary antibody.

Operation of microinjection system

The microinjection system included a microinjector (FemtoJet 4i, Eppendorf) and a micro-manipulator (MS314, WPI) at a step resolution of 0.5 μm. Injected liquid was loaded with a micro-loader (Eppendorf) and then injected into the cells. All the injection process was observed under a charge-coupled device camera (C11440, Hamamatsu), which was a part of the Nikon eclipse Ti-based N-STORM microscopy system.

SUPPLEMENTARY MATERIALS

Supplementary material for this article is available at http://advances.sciencemag.org/cgi/content/full/4/5/eaas9274/DC1

fig. S1. Optimization of the parameters and conditions for high-efficiency 661W cell loading.
fig. S2. A schematic shows the microwell BME-coating process on the NN-Chip.
fig. S3. ROS production, mmp measurements, and SYTOX function test in the blue light–treated 661W cells.
fig. S4. Representative immunostaining images of S-opsin from 0 to 18 hours under blue light irradiation.
fig. S5. Existence of tight junctions in synapses and function validation of the SYTOX.
fig. S6. Apoptotic cells were quantified with or without adjacent apoptotic cells (n = 10).
fig. S7. Generation and verification of Cx36-KO 661W cells.
fig. S8. Calibration of the microinjection volume.
movie S1. Operation of NN-Chip.
movie S2. Three-dimensional structural view of 661W cells cultured onto NN-Chip after 6 hours.
movie S3. Time lapse of the gap junction–mediated bystander killing effect in the 661W cells.
movie S4. Apoptosis propagation from single cell.

REFERENCES AND NOTES

1. A. F. Wright, C. F. Chakarova, M. M. A. El-Aziz, S. S. Bhattacharya, Photoreceptor degeneration: Genetic and mechanistic dissection of a complex trait. *Nat. Rev. Genet.* **11**, 273–284 (2010).
2. A. B. Belousov, J. D. Fontes, Role of neuronal gap junctions in NMDA receptor-mediated excitotoxicity and ischemic neuronal death. *Neural Regen. Res.* **11**, 75–76 (2016).
3. E. Decrock, M. Vinken, E. De Vuyst, D. V. Krysko, K. D'Herde, T. Vanhaecke, P. Vandenabeele, V. Rogiers, L. Leybaert, Connexin-related signaling in cell death: To live or let die? *Cell Death Differ.* **16**, 524–536 (2009).
4. H. Ripps, Cell death in retinitis pigmentosa: Gap junctions and the 'bystander' effect. *Exp. Eye Res.* **74**, 327–336 (2002).
5. K. Cusato, A. Bosco, R. Rozental, C. A. Guimarães, B. E. Reese, R. Linden, D. C. Spray, Gap junctions mediate bystander cell death in developing retina. *J. Neurosci.* **23**, 6413–6422 (2003).
6. P. Kameritsch, N. Khandoga, U. Pohl, K. Pogoda, Gap junctional communication promotes apoptosis in a connexin-type-dependent manner. *Cell Death Dis.* **4**, e584 (2013).
7. C. L. Cepko, The determination of rod and cone photoreceptor fate. *Annu. Rev. Vis. Sci.* **1**, 211–234 (2015).
8. S. Kohl, T. Marx, I. Giddings, H. Jägle, S. G. Jacobson, E. Apfelstedt-Sylla, E. Zrenner, L. T. Sharpe, B. Wissinger, Total colourblindness is caused by mutations in the gene encoding the α-subunit of the cone photoreceptor cGMP-gated cation channel. *Nat. Genet.* **19**, 257–259 (1998).
9. D. C. Spray, R. Hanstein, S. V. Lopez-Quintero, R. F. Stout Jr., S. O. Suadicani, M. M. Thi, Gap junctions and bystander effects: Good Samaritans and executioners. *Wiley Interdiscip. Rev. Membr. Transp. Signal.* **2**, 1–15 (2013).
10. W. Zhang, K. Kai, D. S. Choi, T. Iwamoto, Y. H. Nguyen, H. Wong, M. D. Landis, N. T. Ueno, J. Chang, L. Qin, Microfluidics separation reveals the stem-cell–like deformability of tumor-initiating cells. *Proc. Natl. Acad. Sci. U.S.A.* **109**, 18707–18712 (2012).
11. K. Zhang, C.-K. Chou, X. Xia, M.-C. Hung, L. Qin, Block-Cell-Printing for live single-cell printing. *Proc. Natl. Acad. Sci. U.S.A.* **111**, 2948–2953 (2014).
12. N. Chronis, M. Zimmer, C. I. Bargmann, Microfluidics for in vivo imaging of neuronal and behavioral activity in *Caenorhabditis elegans*. *Nat. Methods* **4**, 727–731 (2007).
13. J. W. Park, B. Vahidi, A. M. Taylor, S. W. Rhee, N. L. Jeon, Microfluidic culture platform for neuroscience research. *Nat. Protoc.* **1**, 2128–2136 (2006).
14. E. Tan, X.-Q. Ding, A. Saadi, N. Agarwal, M. I. Naash, M. R. Al-Ubaidi, Expression of cone-photoreceptor–specific antigens in a cell line derived from retinal tumors in transgenic mice. *Invest. Ophthalmol. Vis. Sci.* **45**, 764–768 (2004).
15. M. Rapp, G. Woo, M. R. Al-Ubaidi, S. P. Becerra, P. Subramanian, in *Retinal Degenerative Diseases* (Springer, 2014), pp. 813–820.
16. L.-p. Yang, X.-. Zhu, M. O. M. Tso, Role of NF-κB and MAPKs in light-induced photoreceptor apoptosis. *Invest. Ophthalmol. Vis. Sci.* **48**, 4766–4776 (2007).
17. J. J. O'Brien, X. Chen, P. R. MacLeish, J. O'Brien, S. C. Massey, Photoreceptor coupling mediated by connexin36 in the primate retina. *J. Neurosci.* **32**, 4675–4687 (2012).
18. A. B. Belousov, J. D. Fontes, Neuronal gap junctions: Making and breaking connections during development and injury. *Trends Neurosci.* **36**, 227–236 (2013).
19. J. C. de Rivero Vaccari, R. A. Corriveau, A. B. Belousov, Gap junctions are required for NMDA receptor–dependent cell death in developing neurons. *J. Neurophysiol.* **98**, 2878–2886 (2007).
20. J. R. Rettig, A. Folch, Large-scale single-cell trapping and imaging using microwell arrays. *Anal. Chem.* **77**, 5628–5634 (2005).
21. L. M. Rapp, S. C. Smith, Morphologic comparisons between rhodopsin-mediated and short-wavelength classes of retinal light damage. *Invest. Ophthalmol. Vis. Sci.* **33**, 3367–3377 (1992).
22. E. I. Azzam, S. M. de Toledo, J. B. Little, Oxidative metabolism, gap junctions and the ionizing radiation-induced bystander effect. *Oncogene* **22**, 7050–7057 (2003).
23. Y. Kuse, K. Ogawa, K. Tsuruma, M. Shimazawa, H. Hara, Damage of photoreceptor-derived cells in culture induced by light emitting diode-derived blue light. *Sci. Rep.* **4**, 5223 (2014).
24. S. G. Jarrett, M. E. Boulton, Consequences of oxidative stress in age-related macular degeneration. *Mol. Aspects Med.* **33**, 399–417 (2012).
25. P. H. Tang, M. C. Buhusi, J.-X. Ma, R. K. Crouch, RPE65 is present in human green/red cones and promotes photopigment regeneration in an in vitro cone cell model. *J. Neurosci.* **31**, 18618–18626 (2011).
26. T. Zhang, N. Zhang, W. Baehr, Y. Fu, Cone opsin determines the time course of cone photoreceptor degeneration in Leber congenital amaurosis. *Proc. Natl. Acad. Sci. U.S.A.* **108**, 8879–8884 (2011).
27. G. R. Juszczak, A. H. Swiergiel, Properties of gap junction blockers and their behavioural, cognitive and electrophysiological effects: Animal and human studies. *Prog. Neuropsychopharmacol. Biol. Psychiatry* **33**, 181–198 (2009).
28. M. Srinivas, M. G. Hopperstad, D. C. Spray, Quinine blocks specific gap junction channel subtypes. *Proc. Natl. Acad. Sci. U.S.A.* **98**, 10942–10947 (2001).
29. E. G. A. Harks, A. D. G. de Roos, P. H. Peters, L. H. de Haan, A. Brouwer, D. L. Ypey, E. J. van Zoelen, A. P. Theuvenet, Fenamates: A novel class of reversible gap junction blockers. *J. Pharmacol. Exp. Ther.* **298**, 1033–1041 (2001).
30. M. Srinivas, D. C. Spray, Closure of gap junction channels by arylaminobenzoates. *Mol. Pharmacol.* **63**, 1389–1397 (2003).
31. E.-J. Lee, J.-W. Han, H.-J. Kim, I.-B. Kim, M.-Y. Lee, S.-J. Oh, J.-W. Chung, M.-H. Chun, The immunocytochemical localization of connexin 36 at rod and cone gap junctions in the guinea pig retina. *Eur. J. Neurosci.* **18**, 2925–2934 (2003).
32. B. Teubner, J. Degen, G. Söhl, M. Güldenagel, F. F. Bukauskas, E. B. Trexler, V. K. Verselis, C. I. De Zeeuw, C. G. Lee, C. A. Kozak, E. Petrasch-Parwez, R. Dermietzel, K. Willecke, Functional expression of the murine connexin 36 gene coding for a neuron-specific gap junctional protein. *J. Membr. Biol.* **176**, 249–262 (2000).
33. A. Calabrese, M. Zhang, V. Serre-Beinier, D. Caton, C. Mas, L. S. Satin, P. Meda, Connexin 36 controls synchronization of Ca^{2+} oscillations and insulin secretion in MIN6 cells. *Diabetes* **52**, 417–424 (2003).
34. J. Rash, W. A. Staines, T. Yasumura, D. Patel, C. S. Furman, G. L. Stelmack, J. I. Nagy, Immunogold evidence that neuronal gap junctions in adult rat brain and spinal cord contain connexin-36 but not connexin-32 or connexin-43. *Proc. Natl. Acad. Sci. U.S.A.* **97**, 7573–7578 (2000).

35. A. J. Kole, E. R. Knight, M. Deshmukh, Activation of apoptosis by cytoplasmic microinjection of cytochrome *c*. *J. Vis. Exp.* e2773 (2011).
36. R. N. Cottle, C. M. Lee, D. Archer, G. Bao, Controlled delivery of β-globin-targeting TALENs and CRISPR/Cas9 into mammalian cells for genome editing using microinjection. *Sci. Rep.* **5**, 16031 (2015).
37. S. A. Bloomfield, B. Völgyi, The diverse functional roles and regulation of neuronal gap junctions in the retina. *Nat. Rev. Neurosci.* **10**, 495–506 (2009).
38. K. Cusato, H. Ripps, J. Zakevicius, D. Spray, Gap junctions remain open during cytochrome c-induced cell death: Relationship of conductance to 'bystander' cell killing. *Cell Death Differ.* **13**, 1707–1714 (2006).
39. J. C. Goldstein, N. J. Waterhouse, P. Juin, G. I. Evan, D. R. Green, The coordinate release of cytochrome c during apoptosis is rapid, complete and kinetically invariant. *Nat. Cell Biol.* **2**, 156–162 (2000).
40. V. Gomez-Vicente, M. Donovan, T. Cotter, Multiple death pathways in retina-derived 661W cells following growth factor deprivation: Crosstalk between caspases and calpains. *Cell Death Differ.* **12**, 796–804 (2005).
41. A. Akopian, T. Atlasz, F. Pan, S. Wong, Y. Zhang, B. Völgyi, D. L. Paul, S. A. Bloomfield, Gap junction-mediated death of retinal neurons is connexin and insult specific: A potential target for neuroprotection. *J. Neurosci.* **34**, 10582–10591 (2014).

Acknowledgments: We thank M. Al-Ubaidi from the University of Houston for providing the 661W cells. **Funding:** We are grateful for funding support from R01 CA180083, R56 AG049714, and R21 CA191179. **Author contributions:** Y.M., X.H., and L.Q. designed research; Y.M., X.H., and B.C.C. performed research; Y.M., B.C.C., P.Z., and K.Z. analyzed data; Y.M., B.C.C., Z.H., and L.Q. wrote the paper. **Competing interests:** The authors declare that they have no competing interests. **Data and materials availability:** All data needed to evaluate the conclusions in the paper are present in the paper and/or the Supplementary Materials. Additional data related to this paper may be requested from the authors. The 661W cell can be provided by M. Al-Ubaidi from the University of Houston pending scientific review and a completed materials transfer agreement. Requests for the 661W cell should be submitted to M. Al-Ubaidi.

Submitted 10 January 2018
Accepted 21 March 2018
Published 9 May 2018
10.1126/sciadv.aas9274

Citation: Y. Ma, X. Han, R. B. de Castro, P. Zhang, K. Zhang, Z. Hu, L. Qin, Analysis of the bystander effect in cone photoreceptors via a guided neural network platform. *Sci. Adv.* **4**, eaas9274 (2018).